

# DESIGN OF A NOVEL CHERENKOV DETECTOR SYSTEM FOR MACHINE INDUCED BACKGROUND MONITORING IN THE CMS CAVERN

Styliani Orfanelli, National Technical University of Athens, Athens- CERN, Geneva, Switzerland

Anne E. Dabrowski, Marina Giunta, CERN, Geneva, Switzerland

David P. Stickland, Princeton University, New Jersey, USA

Mitchell J. Ambrose, Roger Rusack, Alexey Finkel, University of Minnesota, Minnesota, USA

## Abstract

A novel detector system has been designed for an efficient online measurement of the machine-induced background in the CMS experimental cavern. The suppression of the CMS cavern background originating from pp collision products and the 25 ns bunch spacing have set the requirements for the detector design. Each detector unit will be a radiation hard, cylindrical Cherenkov radiator optically coupled to an ultra-fast UV-sensitive photomultiplier tube, providing a prompt, directionally sensitive measurement. Simulation and test beam measurements have shown the achievability of the goals that have driven the baseline design. The system will consist of 20 azimuthally distributed detectors per end, installed at a radius of  $r \sim 180$  cm and a distance 20.6 m away from the CMS interaction region. The detector units will enable a measurement of the transverse distribution of the bunch-by-bunch machine induced background flux. This will provide important feedback from the CMS on the beam conditions during the LHC machine setup and comparisons to expectations based on FLUKA simulations.

## INTRODUCTION AND MOTIVATION

After Long Shutdown 1 (LS1), the Large Hadron Collider (LHC) is expected to exceed the nominal luminosity of  $1.0 \times 10^{34} \text{ cm}^{-2} \text{ s}^{-1}$ , with bunches of intensity  $O(10^{11})$  protons, separated by 25 ns and an energy of up to 6.5 TeV per beam. These operating conditions pose increased risks for the machine protection and poor conditions, which could reduce the quality of the data at the interaction points for the experiments.

The machine-induced background (MIB) refers to particles that arrive in the experiments as a result of adverse beam conditions. The MIB flux consists of secondary particles travelling mostly parallel with the beam and produced either from interactions of beam halo LHC protons at the (tertiary) collimators or beam gas events originating from interaction of primary protons in the vacuum chamber with residual gas atoms. After LS1, such effects could become more critical because of the presence of the electron cloud and the tighter collimator settings imposed by the increased luminosity debris at the triplet at high-luminosity interaction points. It is the responsibility of the CMS experiment to assess the quality of the beam reaching IP5, protect itself from

potentially increased MIB and flag the time intervals with poor beam conditions effecting the data taking quality.

As part of the upgrade of the CMS Beam Radiation Monitoring (BRM) system during LS1, a new detection system will be installed in the CMS cavern, 20.625 m away from the IP, at a radius corresponding to 180 cm from the beam axis, complementing the existing low radius BCM1F detector [1]. The new system aims to measure the beam background arriving from the tunnel, parallel with the incoming beam, and must be able to cope up with the 25ns bunch spacing, be sufficiently radiation hard, sensitive to the MIB and insensitive to the cavern background induced from pp collisions.

## DESIGN REQUIREMENTS

The main purpose of this new beam background system is to provide an online, per bunch, MIB measurement for each of Beam 1 and Beam 2. The properties of the MIB flux, the impact of the CMS cavern environment, the unwanted background rates from collision products and the post-LS1 LHC operating conditions steer the design considerations. The resulting detector requirements are explained in this section:

- excellent time resolution ( $<12.5$  ns)
- directional gain of 1 over 1000
- insensitivity to  $\gamma$  and thermal neutrons
- radiation hard up to 50 krad.



Figure 1: Golden Location 6, the new system will be mounted around the rotating shielding.

## Timing & Choice of location

The MIB flux arriving in CMS can be distinguished from the flux of pp products, which dominate in the cavern, based on their time of arrival. A LHC bunch spacing of 25 ns imposes that the maximum time separation between the two fluxes can be at most 12.5 ns. The locations of the maximum time separation correspond to distances from the IP equal to

ISBN 978-3-95450-127-4

( $6.25+n*12.5$ ) ns,  $n \leq 6$  and are referred to as “Golden Locations”. The detector system should therefore have a response time less than 12.5 ns.

The optimal location for the new background monitoring system was the sixth golden location ( $n=5$ ), which corresponds to ( $6.25+5*12.5$ ) ns, i.e. 20.625 ns, away from the IP, as shown in Fig.1. This choice was made based on the increased absolute MIB flux with respect to other golden locations, the available free space around the rotating shielding and the relatively good environmental conditions (as described in section *Mechanical considerations*).

FLUKA [2] simulation results of the fluxes of all charged particles, with energy above the Cherenkov threshold, arriving at Golden Location 6, induced from both pp collisions (in black) and MIB (in red) as a function of the radial distance from the beam axis, are shown in Fig. 2. The simulation parameters for pp collisions and the arriving MIB fluxes [3] at CMS were the nominal LHC operating settings. Despite the increased absolute MIB flux with respect to other golden locations, the ratio between the MIB and the pp-induced flux at Golden Location 6 is estimated to be  $1/\sim 1000$ .

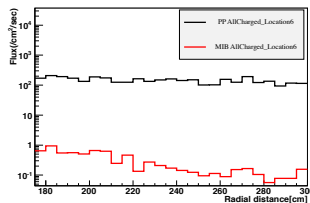


Figure 2: The charged particles fluxes arriving at Golden Location 6 from pp collisions (black) and from MIB (red) as a function of the radial distance from the beam axis.

### Directivity

To suppress the signal contribution of particles originating from the pp collisions, the detector is required to have a directional gain, i.e. an angular response. This angular response could suppress the signal produced by pp products arriving from the opposite direction of the MIB. The MIB flux typically arrives on time with the incoming bunches with a very low rate  $O(\text{Hz}/\text{cm}^2)$  in good operating conditions. A substantial portion of the MIB flux consists of muons arriving at large radius at the CMS experimental area. In Fig. 3a, FLUKA results

show the angular and the energy distribution of the MIB muons arriving at Golden location 6. They travel almost parallel with the incoming beam and with mean energy of a few GeV.

The collision products dominate the rates in the CMS cavern and they are mainly:

- muons which are travelling straight from the IP
- low energy electrons/positrons
- photons and neutrons due to short-term activation of material, so-called ‘albedo’ effect [4].

Angular and energy distributions of the pp muons and the pp electrons/positrons, based on FLUKA simulations, are shown in Fig. 3b and Fig. 3c respectively. The signal produced from the pp muons flux, arriving under very small angle at the opposite direction of the MIB, can be successfully suppressed using a detector with a suitable angular response.

Nevertheless, as shown in Fig. 3c, electrons and positrons arrive from both directions with a larger angular spread, due to multiple scattering effects and secondary interactions. These particles typically have energy less than 100 MeV. Whilst the directional sensitivity would not be able to fully suppress the contribution to the signal from this flux, applying a gating in time and additional shielding (more details in *Mechanical considerations*) have been proposed as a solution.

### Radiation Hardness and Longevity

This system is designed to perform adequately through 10 years of LHC running, for instantaneous luminosity  $1.0 \times 10^{34} \text{ cm}^{-2}\text{s}^{-1}$  and integrated luminosity of  $500 \text{ fb}^{-1}$ . Based on FLUKA simulations, the expected dose in the region of interest is estimated to be less than 5 krad per operating year. Therefore, the raw materials and the detector components were chosen such that their performance doesn’t deteriorate significantly during the lifetime of the system.

## MECHANICAL OPTIMIZATIONS

A Cherenkov based detector satisfies all the previously explained requirements, forming the basis for the detector design. Cherenkov light is inherently directional, prompt and produced only by the interaction of charged particles, making it insensitive to any neutral particles. An ultra-fast photomultiplier tube and a quartz bar as Cherenkov radiator are the main components of this detector system.

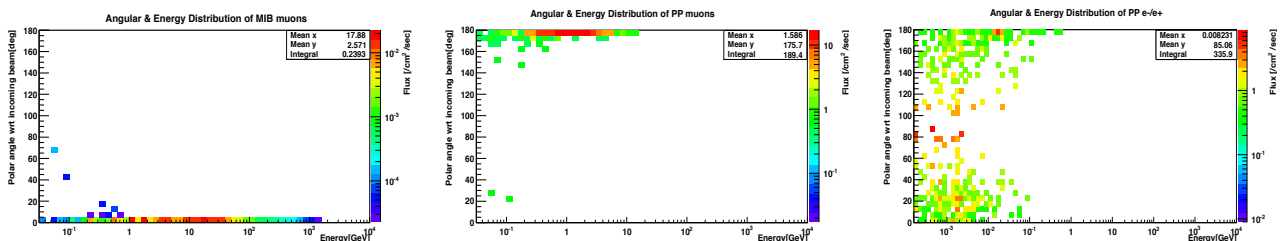


Figure 3: a. MIB muon (left), b. PP muon (middle), c. PP e-/e+ (right) fluxes as a function of the energy (x-axis) and the arriving angle with respect to the incoming beam (y-axis).

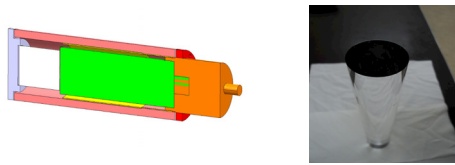


Figure 4: The drawing of the detector unit (left) and a quartz bar used during the test-beams (right).

The drawing of Fig. 4 shows a detector unit composed by a quartz bar (white), coupled to a PMT (green) all shielded by 0.5 cm of soft iron (pink). The front face (purple) is an aluminum cap. The front side of the quartz bar is black painted, while from the other side there is an optical material used to couple the quartz bar to the PMT. Along this section the choice of each of the components is explained.

### Choice of material and components

Cherenkov radiation emission spectrum is continuous and more intense in shorter wavelengths. Therefore, components that would be able to transmit light in the UV area, even after receiving the expected dose, were chosen. Various quartz samples (Heraeus) were irradiated to twice the expected dose, 100 krad with a  $Co^{60}$  source emitting  $\sim 1MeV$   $\gamma$  rays. In Figure 5, the blue dotted line shows how the transmission coefficient of electrically fused quartz HSQ330 deteriorates after irradiation with respect to the one before (continuous blue). No significant deterioration was observed for the synthetic quartz Suprasil (in orange), which is the reason, this type of fused silica produced in a fully synthetic production process was the material of choice. In the same plot, the respective results from two different optical coupling samples (Biesterfeld), irradiated with 100 krad dose, are shown. In green are presented the results for optical glue RTV3145 (and in black, for optical gel DC93-500). No change after irradiation was observed for either optical coupling. Both materials are currently under consideration and the final choice shall be defined by the ease of usage during the assembly of the detector units.

The most suitable photodetector in terms of fast response ( $\ll 12.5ns$ ), UV sensitivity and large surface sensitive area to increase as possible the acceptance of the low MIB rate, is the Hamamatsu R2059. The diameter of the quartz bar was chosen to match the PMT window i.e. 51mm.

Geant4 [5] simulations were performed to decide on the optimal length for the Cherenkov radiator. Specifically, the variation of the number of Cherenkov photons arriving at the photocathode as a function of the polar angle of an impacting 4 GeV muon was studied. The length of the radiator was varying between 2 cm to 20 cm and its diameter was, in all cases, 51 mm. The number of photons for a length  $l$  and an impact angle  $\varphi$ , normalized to the average number of photons of each length case,

\* <http://www.heraeus.com/>  
 \*\* <http://www.biesterfeld.com/>  
 \*\*\* <http://www.hamamatsu.com/>

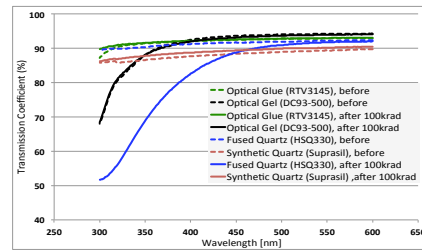


Figure 5: Transmission coefficient of optical materials, before (dotted) and after (continuous) 100 krad irradiation with  $\gamma$  rays ( $E \sim 1MeV$ ) using a source  $Co^{60}$ .

defines the directional gain of the radiator. In Fig. 6, the directional gain for bars of 2 cm (pink), 6 cm (yellow), 10 cm (green), 14 cm (blue) and 20 cm (red) is depicted. Directivity, defined as the maximum of the directional gain of the radiator, corresponds to the directional gain of 0 deg. As the radiator length is shortened, the directivity deterioration and the presence of ‘side-lobes’ become significant. The length of 10 cm was decided, as the best balance between directivity and compactness, having sufficiently large signal response to treat in the readout chain.

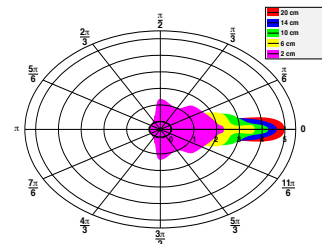


Figure 6: Directional gain for various lengths of radiator.

### Shielding

As previously explained, one of the arguments for the choice of Golden Location 6 for the installation of the new background monitoring system was the availability of the space and the relatively good environmental conditions. Standing 20 m away from the IP has the optimal effect of shielding from the majority of the collision products, the radiation dose and the CMS magnetic field by the CMS detector itself.

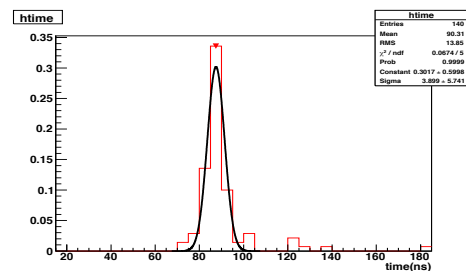


Figure 7: Time of arrival of the fake signal with respect to the time of collision ( $t=0ns$ ).

However, there is still a presence of <200 gauss of magnetic field and the low energetic electrons/positrons from pp collisions arriving from the same direction with the MIB flux, composing the “fake signal” component. To protect the PMT from the magnetic field a soft iron shielding will cover the assembled detector unit. This soft iron tube of 5 mm thickness and 24 cm length would suppress both the magnetic field inside the unit and the fake signal contribution. The presence of 5 mm iron suppresses the signal induced by  $e^-/e^+$  below 10 MeV (90% of the fake signal). The 90% of the rest of it arrives in a time window of 10 ns (Fig. 7), allowing a final suppression of the total fake signal flux to 1%, by using gating in time.

## DESIGN VALIDATION

The front-end design of this detector was tested at various CERN test beam lines during 2012 to verify assumptions about the response time and directivity of the detector components. In Fig. 8a, the fast timing distribution of the signal, when using the R2059 PMT during a test beam in T9 in July 2012, is shown. The set up (Fig. 8b) consisted of a quartz bar directly coupled to the PMT and the trigger was based on the coincidence of three scintillators that were placed before and after the detector unit.

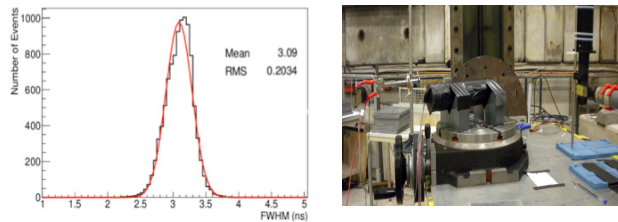


Figure 8: a. The FWHM of 3.1 ns (left). b. The test beam setup during July 2012 (right).

The directional response of the detector was studied in detail during December 2012 in a test beam in T9 with identical setup, with the addition of an optical coupling between the radiator and the PMT. Figure 9a shows the amplitude distribution for incoming particles arriving under 0 deg and 180 deg. Figure 9b is an accumulative plot of Fig. 9a of the backward particle amplitude distribution and an inversed accumulative plot of the forward particle amplitude distribution. By setting a discrimination voltage such that 95% of the forward signal is accepted, the backward signal acceptance is suppressed to  $O(10^{-3})$ , achieving the required 0.1% suppression of the signal induced by pp products, by rejecting only 5% of the signal coming from MIB.

## SYSTEM OVERVIEW

In Fig. 10a the distribution in the x-y plane of the MIB flux arriving at Golden Location 6 is shown. Notice the higher flux in the horizontal plane, which is a characteristic of the beam and the way it is treated before it arrives at the CMS. The rate of MIB arriving at the

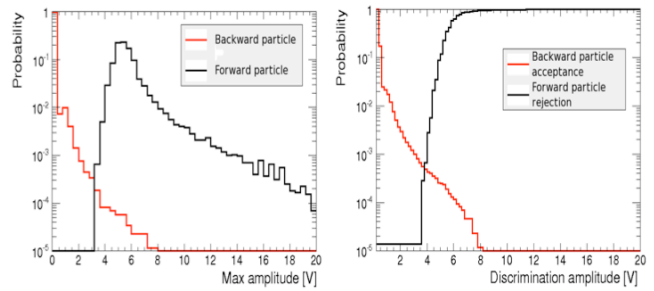


Figure 9: a) Normalized amplitude distribution (left). and b) accumulative distribution (right) of signal from forward particle (black) and backward particle (red).

detector location and the goal of providing a bunch-by-bunch measurement set the requirement of a total acceptance of  $400 \text{ cm}^2$ . With the geometrical acceptance of a detector unit equal to  $20.4 \text{ cm}^2$ , twenty channels per end was decided to be distributed azimuthally around the rotating shielding, having an overlapping acceptance with the CMS muon chambers. In Figure 10b, the mechanical drawings of the structure that will support the detector units are shown.

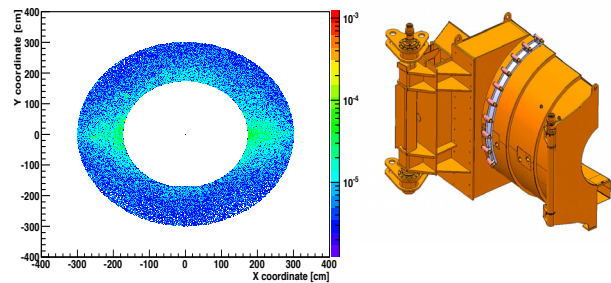


Figure 10: a. Normalized MIB distribution in x-y plane (left). b. Mechanical drawing of a quarter of the system (right).

## OUTLOOK

A novel Cherenkov-based beam background system has been designed with key features, the fast timing and the directional gain, and will be installed in CMS during LS1.

## REFERENCES

- [1] N. Odell, "Measurements of Luminosity and Normalised Beam-Induced Background Using the CMS Fast Beam Condition Monitor" ICHEP2012, Melbourne, Australia, PoS (ICHEP 2012) 526
- [2] A. Ferrari, et al., "FLUKA: a multi-particle transport code" CERN-2005-10 (2005), INFN/TC\_05/11, SLAC-R-773
- [3] N.V. Mokhov, et al., "Machine-Induced Backgrounds: Their Origin and Loads on ATLAS/CMS", Fermilab-Conf-08-147-APC, May (2008)
- [4] S. Mueller, "The Beam Condition Monitor 2 and the Radiation Environment of the CMS Detector at the LHC", CERN-THESIS-2011-085
- [5] S. Agostinelli, et al., "Geant4 - a Simulation Toolkit" Nucl. Instrum. Meth. A, vol. 506, no. 3, pp. 250-303, (2003)